JOURNAL OF MAGNETIC RESONANCE **130,** 176–185 (1998)
ARTICLE NO. MN971311

High-Speed Magic-Angle Spinning ^{13}C MAS NMR Spectra of Adamantane: Self-Decoupling of the Heteronuclear Scalar Interaction and Proton Spin Diffusion

Matthias Ernst, Aswin Verhoeven, and Beat H. Meier

NSR-Center for Molecular Structure, Design, and Synthesis, Laboratory of Physical Chemistry, University of Nijmegen, Toernooiveld 1, NL-6525 ED Nijmegen, The Netherlands

Received July 1, 1997

We have investigated the carbon line shape of solid adamantane under high-speed magic-angle sample spinning (MAS) acquired without proton decoupling. The CH-group shows a spinning-speed-dependent line broadening while the CH_2-group consists of a spinning-speed-independent sharp component and a spinning-speed-dependent broader part. These phenomena can be explained by self-decoupling of the *J*-interaction due to proton spin diffusion. Such a self-decoupling process can be described by a magnetization exchange process between the multiplet lines. Changing the spin-diffusion rate constant by off-resonance irradiation of the protons allows us to observe the full range from slow exchange to coalescence to fast exchange of the carbon spectra. One of the multiplet components in the CH_2-group corresponds to a group spin of the protons of zero and therefore does not couple to the other protons. This gives rise to the sharp central line. The magnetization exchange rate constant between the different multiplet lines can be determined from the spectra and is a measure for the spinning-speed-dependent proton spin-diffusion rate constant. Even at an MAS speed of 30 kHz, proton spin diffusion is still observable despite the relatively weak intermolecular proton dipolar-coupling network in adamantane which results in a static proton line width of only 14 kHz (full width at half height).

Key Words: **solid-state NMR; spin-diffusion; MAS; self-decoupling.**

INTRODUCTION

The ^{13}C-spectrum of a solid with spin-1/2 nuclei under fast magic-angle spinning (MAS) (*1–3*) is expected to approach the liquid-state spectrum. Here, ''fast'' refers to the situation where the MAS frequency greatly exceeds the size of the largest interaction in the system Hamiltonian. For adamantane ($C_{10}H_{16}$), a plastic crystal with considerable internal motion, the largest interaction in the spin system is the intermolecular ^1H homonuclear dipolar coupling with an (orientation-dependent) maximum size of $\omega_D^{(H)} = \mu_0/(4\pi)\cdot\gamma_H^2\hbar/r_{HH}^3 = 2\pi\cdot 420$ Hz leading to a static proton line width of about 13,800 Hz (full width at half height). Nevertheless, the undecoupled ^{13}C-spectrum under MAS at 30 kHz, the fastest rate available to us, does still not lead to a ''liquid-like'' spectrum with a 1:2:1 *J*-splitted triplet for the CH_2 group and a 1:1 doublet for the CH group (Fig. 1). The scalar heteronuclear couplings, measured in the liquid state, are $J_{CH} = 131$ Hz and $J_{CH_2} = 126$ Hz (*4*).

Figure 1 shows the experimental ^{13}C spectra of solid adamantane as a function of the spinning speed ranging from $\nu_r = \omega_r/(2\pi) = 10$ to 30 kHz. The CH-group shows at all speeds a single line but the line becomes significantly broader at higher speeds with some indications of a multiplet splitting at the highest MAS frequency. The CH_2-group appears to be a single line at lower spinning speeds ($\nu_r = 10$ and 15 kHz) but at higher speeds ($\nu_r > 15$ kHz) the line shape appears to be a superposition of a sharp line in the center of the peak and a quite broad line. A closer investigation reveals the presence of a sharp component for all five spinning speeds. The line width of the sharp component is largely independent of the spinning speed while the broad component broadens significantly with higher spinning speed.

The expected doublet and triplet structure can be observed, however, in the presence of homonuclear proton decoupling (*5–8*) or in isotopically diluted samples (5% protonated adamantane in 95% perdeuterated adamantane, ^{13}C in natural abundance (*9*)). These observations suggest that the line shapes of the spectra in Fig. 1 are a manifestation of ''self-decoupling'' of the heteronuclear *scalar* coupling by the proton spin-diffusion process (*10*). ''Self-decoupling'' processes of the heteronuclear *dipolar* interaction have been described for a number of systems (*11–15*). As detailed below, the magnetization exchange between the proton spins caused by the proton spin-diffusion process manifests itself in the carbon spectrum like a ''chemical exchange'' process (*16*) and can be described by Bloch-type equations modified for exchange (*17*). If the spin-diffusion rate constant is much smaller than the *J*-interactions, well-resolved *J*-multiplets are predicted; if the spin-diffusion rate constant rivals the *J*-interaction, coalescence of the multiplet

1090-7807/98 $25.00

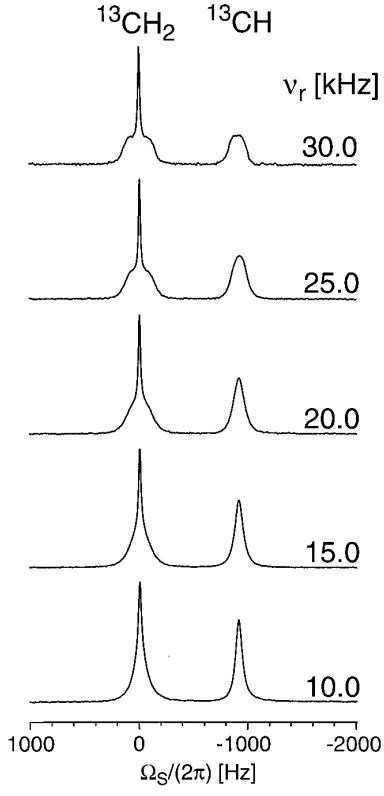

FIG. 1. Carbon spectra of adamantane with natural isotopic abundance at five different spinning speeds from $\nu_r = 10$ to 30 kHz recorded without proton decoupling. The CH-group shows a spinning-speed-dependent line broadening which is due to the magnetization exchange between the two lines of the *J*-multiplet mediated by proton spin diffusion. The CH_2-group also shows this exchange broadening but has in addition a sharp line in the center which does not change with spinning speed.

line is observed and for fast spin diffusion a single sharp line is expected. Through a scaling of the homonuclear *I*-spin dipolar interaction using off-resonance rf-irradiation (*18*), the transition from ''slow exchange'' to ''fast exchange'' can be observed experimentally in adamantane as described in this article.

By fitting the carbon spectra with a suitable exchange model, we were able to determine exchange rate constants (proton spin-diffusion rate constants) in the presence of fast MAS. A related scheme for indirect detection of the proton spin-diffusion process in adamantane, based on 2D-exchange spectroscopy (*19, 20*), has been applied by Takegoshi and McDowell (*8*) in the slow-spinning regime (spinning speed $\nu_r = 2.6$ kHz), where the multiplet lines are not resolved in the one-dimensional spectrum but can still be resolved under homonuclear multiple-pulse decoupling (MREV-8) (*21*).

THEORY

In adamantane, the fast pseudo-isotropic rotation of the molecule (with a correlation time at room temperature of $\tau_c \approx 1.6 \times 10^{-11}$ s (*22, 23*)) averages out all intramolecular dipolar interactions (homo- and heteronuclear) as well as the chemical-shielding anisotropy. We may, therefore, write the system Hamiltonian as

$$H \approx H_{\text{intra}}^{(\text{CH})} + H_{\text{intra}}^{(\text{CH}_2)} + H_{\text{rf}}^{(\text{CH})} + H_{\text{rf}}^{(\text{CH}_2)} + H_{\text{II}}(t) + H_{\text{SI}}(t) + H_{\text{SS}}(t), \quad [1]$$

with the intramolecular contributions

$$H_{\text{intra}}^{(\text{CH})} = \Omega_{1S} \cdot S_{1z} + \Omega_{1I} \cdot I_{1z} + 2\pi J_{\text{CH}} \cdot S_{1z} I_{1z} \quad [2]$$

and

$$H_{\text{intra}}^{(\text{CH}_2)} = \Omega_{2S} \cdot S_{2z} + \Omega_{2I} \cdot I_{2z} + \Omega_{3I} \cdot I_{3z} + 2\pi J_{\text{CH}_2} \times S_{2z}(I_{2z} + I_{3z}) + 2\pi J_{\text{HH}} \cdot \vec{I}_2 \cdot \vec{I}_3, \quad [3]$$

where the Ω_{nS} denote *S*-spin (^{13}C) isotropic chemical shifts and the Ω_{nI} represent *I*-spin (^{1}H) isotropic chemical shifts (measured with respect to the respective rf carrier frequencies). J_{CH} and J_{CH_2} describe the heteronuclear scalar couplings, and J_{HH} describes the homonuclear scalar coupling between the two protons of a $^{13}CH_2$-group. Long-range proton scalar couplings and the scalar couplings between rare spins are neglected.

The interaction with the radio-frequency field (for the case of an off-resonance rf-irradiation) applied to the protons is given by

$$H_{\text{rf}}^{(\text{CH})} = \omega_{\text{rf}} I_{1x} \quad [4]$$

and

$$H_{\text{rf}}^{(\text{CH}_2)} = \omega_{\text{rf}}(I_{2x} + I_{3x}). \quad [5]$$

The remaining three terms in Eq. [1] contain only intermolecular interactions. The intermolecular proton homonuclear coupling, explicitly time dependent due to MAS, is given by

$$H_{II}(t) = \sum_{i<j} \omega_{ij}(t) \cdot \left(2I_{iz}I_{jz} - \frac{1}{2}(I_i^+ I_j^- + I_i^- I_j^+) \right), \quad [6]$$

where the indices *i* and *j* extend over all protons in the sample. Therefore, $H_{II}(t)$ potentially can lead to a coupling of the CH and CH_2 spin systems that evolve independently under the four leading terms of Eq. [1]. Because the *S*-spins are rare, we may assume, however, in reasonable approximation that during the time of the free-induction decay each *S*-spin interacts only with a limited set of close-by *I*-spins. This implies that no *I*-spins are ''shared'' between two *S*-

spin systems. Similar arguments can be made for the intermolecular heteronuclear dipolar coupling

$$H_{SI}(t) = \sum_{i,j} \omega_{ij}(t) \cdot 2I_{iz}S_{jz}. \quad [7]$$

The homonuclear *S*-spin Hamiltonian $H_{SS}(t)$ can be neglected because the *S*-spins are rare and the Hamiltonian is, therefore, very small. Under these conditions, the CH and CH_2 spin systems remain separated and the respective Hamiltonians commute.

The time-dependent Hamiltonian of Eq. [6] shall be treated in average Hamiltonian theory (AHT) (*24–26*) to describe the averaging by the off-resonance irradiation and the magic-angle sample spinning as two consecutive averaging processes. Such an approach is allowed if the time scales of the two processes are different which is the case if $\omega_{rf} \gg \omega_r$. If we subject the system to an off-resonance rf-irradiation on the protons, it is convenient to transform the system Hamiltonian into a tilted rotating frame where the quantization axis is along the effective field for the protons. Assuming that the variation in the offset frequencies of the protons is small, the tilt angle of this reference frame is the same for all protons and is given by

$$\theta \approx \arctan\left(\frac{\omega_{rf}}{\Omega_{nI}}\right). \quad [8]$$

In such a frame, all heteronuclear interactions scale (in zeroth-order approximation) with $\cos\theta$, while the *S*-spin part of the Hamiltonian is unaffected. The homonuclear dipolar Hamiltonian of Eq. [6] scales as a second-rank spin tensor

$$H_{II}^{\theta}(t) = P_2(\cos\theta) \cdot H_{II}(t). \quad [9]$$

In a second averaging process we can treat the mechanical sample rotation also by average Hamiltonian theory. Due to the second-rank properties of the spatial part of the homonuclear and the heteronuclear dipolar interaction, the zeroth-order term vanishes over a full rotor period with $t_c = 2\pi/\omega_r$,

$$\bar{H}_{II}^{(0)} = \frac{1}{t_c}\int_0^{t_c} H_{II}^{\theta}(t_1)dt_1 = 0, \quad [10]$$

and

$$\bar{H}_{SI}^{(0)} = 0. \quad [11]$$

The first-order term of the dominant intermolecular interaction $H_{II}(t)$ leads to

$$\bar{H}_{II}^{(1)} = \frac{-i}{2t_c}\int_0^{t_c} dt_2 \int_0^{t_2} [H_{II}^{\theta}(t_2), H_{II}^{\theta}(t_1)]dt_1$$

$$= -\frac{i}{\omega_r} \cdot P_2(\cos\theta)^2 \sum_{i\neq j\neq k} \omega'_{ijk} I_{i,z}(I_j^+ I_k^- - I_j^- I_k^+), \quad [12]$$

where ω'_{ijk} depends on the dipolar-coupling network (distances and angles) but not on the rotation speed. While the form of $\bar{H}_{II}^{(1)}$ differs from the one of the static dipolar interaction, H_{II}, it still causes proton flip-flop processes.

The two consecutive averaging processes lead to an average Hamiltonian for the CH and CH_2 group given by

$$\bar{H}^{(CH)} = \Omega_{1S} \cdot S_{1z} + 2\pi J_{CH}^{\theta} \cdot S_{1z}I_{1z} - \frac{i}{\omega_r} \cdot P_2(\cos\theta)^2 \sum_{i\neq j\neq k} \omega'_{ijk} I_{i,z}(I_j^+ I_k^- - I_j^- I_k^+) \quad [13]$$

and

$$\bar{H}^{(CH_2)} = \Omega_{2S} \cdot S_{2z} + 2\pi J_{CH_2}^{\theta} \cdot S_{2z}(I_{2z} + I_{3z}) - \frac{i}{\omega_r} \cdot P_2(\cos\theta)^2 \sum_{i\neq j\neq k} \omega'_{ijk} I_{i,z}(I_j^+ I_k^- - I_j^- I_k^+) + 2\pi J_{HH} \cdot \vec{I}_2 \cdot \vec{I}_3, \quad [14]$$

with $J_{CH}^{\theta} = \cos\theta \cdot J_{CH}$ and $J_{CH_2}^{\theta} = \cos\theta \cdot J_{CH_2}$. For the CH-group the first two terms of the Hamiltonian of Eq. [13] lead to a carbon spectrum with two resonances which one can identify as a ^{13}C having a proton spin in its $|\alpha\rangle$ or $|\beta\rangle$ state as binding partner, respectively. The third term in the Hamiltonian introduces transitions from $|\alpha\rangle$ to $|\beta\rangle$ for the *I*-spins because it does not commute with I_{1z}. For an extended proton coupling network, the jumps from $|\alpha\rangle$ to $|\beta\rangle$ will appear quite randomly and, formally, this situation is identical to a chemical exchange process between two sites with resonance frequencies $\Omega_{CH} \pm \pi J_{CH}^{\theta}$ occurring at a rate constant of k_0 (see also Fig. 2). The last term in Eq. [14] can be neglected, as it does not influence the spectrum.

We can describe the exchange process by the modified Bloch equations (*17*). The line positions are given by the complex part of the eigenvalues of the spectral matrix

$$\begin{bmatrix} -k_0 - \frac{\pi}{T_2^{CH}} + i(\Omega_{1S} + \pi J_{CH}^{\theta}) & k_0 \\ k_0 & -k_0 - \frac{\pi}{T_2^{CH}} + i(\Omega_{1S} - \pi J_{CH}^{\theta}) \end{bmatrix}. \quad [15]$$

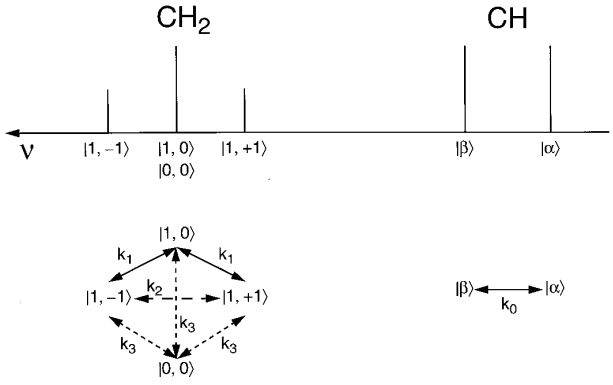

FIG. 2. Schematic *J*-coupled carbon spectrum of adamantane with an assignment of the proton states to the different multiplet lines. In addition, the relevant exchange-rate constants are indicated which connect the different proton states.

the line width by the real part. Here, T_2^{CH} is the transverse relaxation time in the absence of the exchange process. For $k_0 \ll 2\pi J^{\theta}_{CH}$ the *S*-spin spectrum consists of two lines separated by the dipolar-coupling constant $2\pi J^{\theta}_{CH}$. With increasing k_0 the lines start to broaden. At $k_0 = \pi J^{\theta}_{CH}$, the two line positions become degenerate (due to the width of the lines, coalescence appears already at $k_0 = kJ^{\theta}_{CH_2}/\sqrt{2}$) and, on further increasing k_0, the resulting single line narrows again. Because k_0 is the proton–proton flip-flop rate constant, we may talk of ''self-decoupling'' for $k_0 \gg \pi J^{\theta}_{CH}$.

For the CH_2-group we use a symmetry-adapted basis reflecting the magnetic equivalence of the two protons (*27*). Use of the symmetry-adapted basis functions is mandated by the fact that the single-spin quantum numbers are no longer good quantum numbers due to the equivalence of the two protons. The symmetry-adapted basis functions are

$$\begin{aligned} |\alpha, \alpha\rangle &= |1, +1\rangle \\ 1/\sqrt{2}(|\alpha, \beta\rangle + |\beta, \alpha\rangle) &= |1, 0\rangle \\ 1/\sqrt{2}(|\alpha, \beta\rangle - |\beta, \alpha\rangle) &= |0, 0\rangle \\ |\beta, \beta\rangle &= |1, -1\rangle, \end{aligned} \qquad [16]$$

where the notation on the right-hand side refers to the group spin quantum number F and the magnetic quantum number F_z, $|F, F_z\rangle$. Only states with $F = 1$ (''pseudo-spin-1'') experience a homonuclear dipolar coupling to other protons in the sample and participate, therefore, in the proton spin-diffusion process. The $F = 0$ (''pseudo-spin-0'') state does not couple to the other protons. This behavior has important consequences for the exchange narrowing visible in the carbon spectrum. Figure 2 shows the four states and the possible transitions in the CH_2-group. However, not all possible transitions in the CH_2-group happen with a high probability. The pathways $|1, +1\rangle \leftrightarrow |1, 0\rangle$ and $|1, -1\rangle \leftrightarrow |1, 0\rangle$ have a high probability because they correspond to a simultaneous flip-flop of the pseudo-spin-1 with another spin in the sample, either a spin-1/2 from a CH-group or a pseudo-spin-1 from a CH_2-group. Both processes are promoted by the homonuclear first-order Hamiltonian of Eq. [12].

Analogous to the CH-group, we can also find the line positions and line widths of the carbon resonances of the $^{13}CH_2$-group from the eigenvalues of the spectral matrix using the symmetry-adapted pseudo-spin-1 basis for the proton states

$$\begin{bmatrix} -(k_1 + k_2) - \frac{\pi}{T_2^{CH_2}} + i(\Omega_{2S} + 2\pi J^{\theta}_{CH_2}) & k_1 & k_2 \\ k_1 & -2k_1 - \frac{\pi}{T_2^{CH_2}} + i\Omega_{2S} & k_1 \\ k_2 & k_1 & -(k_1 + k_2) - \frac{\pi}{T_2^{CH_2}} + i(\Omega_{2S} - 2\pi J^{\theta}_{CH_2}) \end{bmatrix}. \qquad [17]$$

We expect the rate constant k_1 to be the dominant process over k_2 which is associated with the forbidden $|1, -1\rangle \leftrightarrow |1, +1\rangle$ transition. Double-quantum spin diffusion in spin-1 systems occurs only if the second-order perturbation treatment fails and fourth-order terms become important (*28*). By diagonalizing the matrix in Eq. [17], one finds that a common frequency for the three lines of the pseudo-spin-1 system appears at $k_1 \approx 1.54 \cdot 2\pi J^{\theta}_{CH}$. The pseudo-spin-0 gives rise to a single resonance line at ω_{CH_2}.

According to Abragam (*29*), the rate constant for a transition between state $|m\rangle$ and $|m - 1\rangle$ of a spin with quantum number I under a perturbation of strength ω_1 is given by

$$W_{m,m-1} = \frac{\pi}{2} \cdot \omega_1^2 \cdot (I + m) \cdot (I - m + 1) \cdot f(\omega). \qquad [18]$$

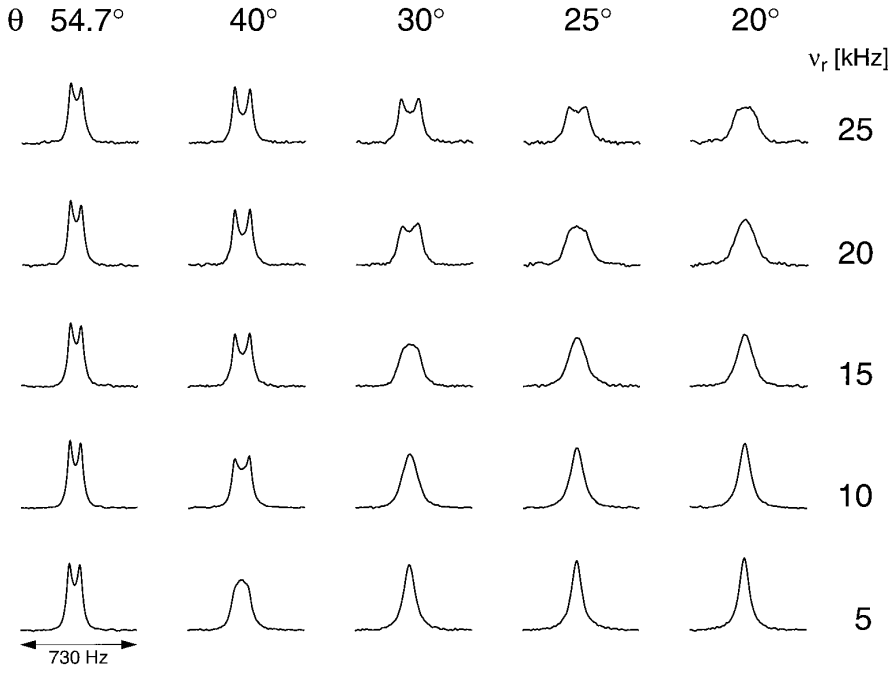

FIG. 3. Carbon spectra of the CH-group of adamantane for five different spinning speeds in the range from $\upsilon_r = 5$ to 25 kHz and under off-resonance proton decoupling. The angle of the effective proton field with the z-axis, θ, varies between $\theta = 54.7°$ (the magic angle) and $\theta = 20°$. The effective J-coupling in these spectra scales with $\cos\theta$ while the homonuclear dipolar coupling, which is responsible for the exchange process between the multiplet lines, scales with $P_2(\cos\theta)$. Near the magic angle ($\theta = \arccos(1/\sqrt{3})$), the J-multiplets are resolved at all spinning speeds. At smaller angles the exchange process between the multiplet lines becomes faster, leading to a collapse of the multiplets at lower spinning speed.

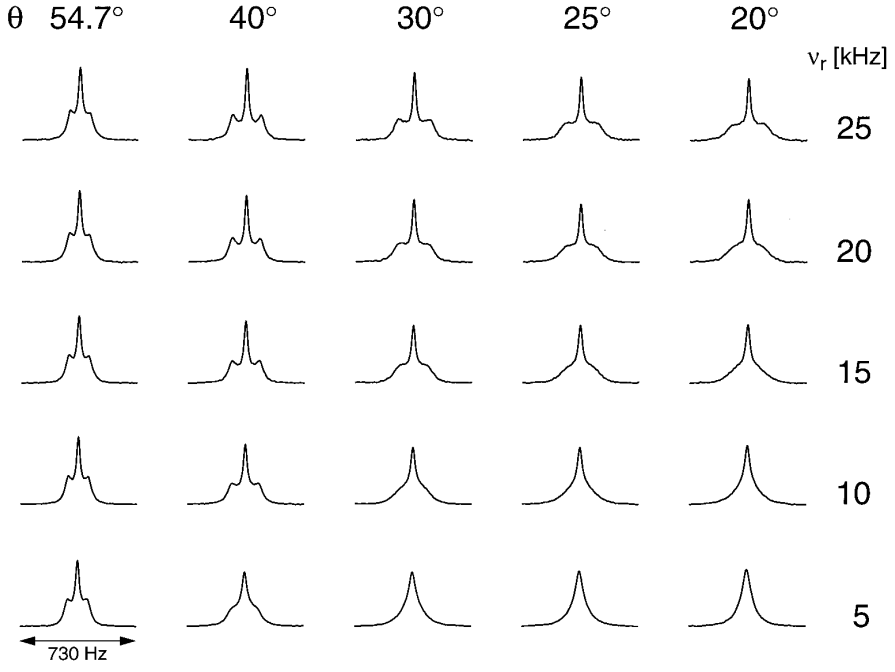

FIG. 4. Carbon spectra of the CH_2-group of adamantane for five different spinning speeds in the range from $\upsilon_r = 5$ to 25 kHz and under off-resonance proton decoupling. The angle of the effective proton field with the z-axis, θ, varies between $\theta = 54.7°$ (the magic angle) and $\theta = 20°$. The CH_2-group shows a sharp central peak with a line width independent of the spinning speed and the effective field direction. The other multiplet lines show an analogous behavior due to the proton magnetization exchange process as described in Fig. 3 for the CH-group.

For a spin $I = 1/2$ this leads to the transition probability

$$W_{1/2,-1/2} = k_0 = \frac{\pi}{2} \cdot \omega_1^2 \cdot f(\omega), \qquad [19]$$

while for a spin $I = 1$ the probability is

$$W_{1,0} = W_{0,-1} = k_1 = \pi \cdot \omega_1^2 \cdot f(\omega) = 2 \cdot k_0, \qquad [20]$$

twice as large as for the spin-1/2 case. In our case the perturbation ω_1 is proportional to the first-order dipolar-coupling constant of Eq. [12] and $f(\omega)$ is the zero-quantum line intensity at frequency zero (*28*). The first-order dipolar-coupling constant of Eq. [12] (and therefore ω_1) scales with $P_2(\cos\theta)^2$ and ω_r^{-1} while the intensity of the zero-quantum line scales, in a rough approximation, inversely with the Hamiltonian, i.e., with $P_2(\cos\theta)^{-2}$ and ω_r. We expect, therefore, the rate constant $W_{m,m-1}$ to be scaled by $P_2(\cos\theta)^2$ and by ω_r^{-1}. The ratio of the transition probabilities $k_1 = 2 \cdot k_0$ can also be seen from the dipolar-coupling Hamiltonian written in the symmetry-adapted basis. The off-diagonal elements describing the flip-flop terms are by a factor of $\sqrt{2}$ larger for the coupling of the pseudo-spin-1 system of the CH_2-group with a spin-1/2 system compared to the coupling between two spin-1/2 systems. Consequently, the flip-flop terms for the coupling of two pseudo-spin-1 systems lead to a factor of 2 larger off-diagonal element.

Due to the properties of a spin-0 system, the state $|0, 0\rangle$ cannot undergo simultaneous spin flips with another spin mediated through a direct dipolar coupling. There is, however, the possibility of cross relaxation between the spin-1 states and the spin-0 states of the two protons in the CH_2-group. It is well known that in solid adamantane the main relaxation pathway is due to the modulation of the dipolar couplings by the fast reorientation of the molecules (*22, 23*). Based on the normal-mode representation of longitudinal relaxation in an AX_2 spin system (*30–32*) we can estimate the cross-relaxation rate constant between the $F = 0$ and the $F = 1$ states for an isotropic rotation of the adamantane molecule with a correlation time of $\tau_c \approx 1.6 \times 10^{-11}$ s to be $k_3 \approx 0.4\ s^{-1}$.

As mentioned before, we have only considered the homonuclear dipolar terms in the first-order average Hamiltonian treatment (see Eq. [12]). In principle, cross terms between the heteronuclear dipolar coupling $H_{SI}(t)$ and the homonuclear dipolar coupling $H_{II}(t)$ also exist. Because of their smaller amplitude and because of the isotopic dilution of the *S* spins, these cross terms can be neglected for the calculation of the proton spin-diffusion rate constant. These terms render the heteronuclear dipolar coupling homogeneous under MAS and can lead to a general broadening of all the multiplet components of the carbon spectrum which can be included in the relaxation-induced line width. The high-speed spectra are, however, only weakly influenced by this broadening because the lifetime of the proton spin states is always long compared to the inverse of the spinning speed. In contrast, the exchange broadening of the *J*-coupled lines, as described above, is sensitive to proton-state lifetimes in the order of the inverse of the scalar *J*-coupling, which is 200 times smaller than the fastest spinning speeds.

RESULTS AND DISCUSSION

Figures 3 and 4 show a series of directly excited one-dimensional carbon spectra for spinning speeds between $\upsilon_r = 5$ kHz and $\upsilon_r = 25$ kHz and for angles of the effective quantization axis of the protons with the magnetic field between $\theta = 20°$ and 54.7° (''Lee–Goldburg'' irradiation) (*18, 26*). Experimental details are given in the Appendix. At the magic angle ($\theta = \arccos(1/\sqrt{3})$) where $P_2(\cos\theta) =$

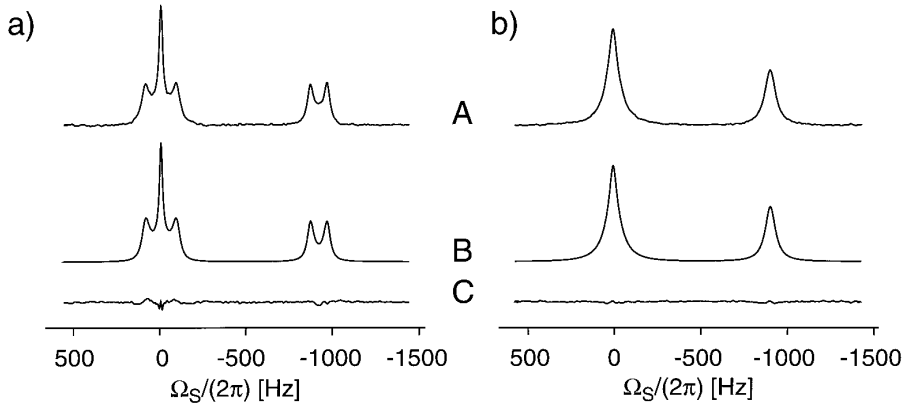

FIG. 5. Two representative experimental carbon spectra ((a) $\upsilon_r = 25$ kHz, $\theta = 40°$; (b) $\upsilon_r = 5$ kHz, $\theta = 20°$) from Figs. 3 and 4 (A) together with the best computer fit (B) using the exchange model discussed in the text and the residual (C). The same level of good agreement between measurements and the exchange simulation was achieved for all spectra.

0, the homonuclear flip-flop term in the first-order Hamiltonian for the CH and the CH_2 groups vanishes and $k_0 = k_1 = 0$. The CH and CH_2 resonances should consist of a doublet and a 1:2:1 triplet, respectively, independent of the MAS rate. Approximately, this behavior is indeed observed in the first column of Figs. 3 and 4. The central component of the triplet (Fig. 4) is, however, still narrower than the satellites, indicating that the LG irradiation does not perform ideally. The remaining line broadenings are probably due to rf-field inhomogeneities and to higher-order terms in the average Hamiltonian expansion. At smaller values of θ, the influence of the spinning speed on the spectra becomes much more pronounced. At $\theta = 30°$, for example, the appearance and breakdown of the self-decoupling are clearly seen in the spectra of the CH-group (Fig. 3) for spinning speeds between 5 and 25 kHz. At 5 kHz, a single ''self-decoupled'' line is observed; at about 15 kHz coalescence occurs; and at 25 kHz, a *J*-coupled multiplet with a *J*-splitting of $\sim 0.86 \cdot J_{CH}$ is observed. At smaller angles θ coalescence moves to higher spinning speeds; at $\theta = 0$ (no proton irradiation, see Fig. 1) coalescence seems to occur around the highest spinning speed of 30 kHz. It is important to remember that with decreasing angle θ the apparent *J*-coupling increases because the *J*-coupling scales with $\cos\theta$. The same behavior is visible in the three lines of the CH_2-multiplet (Fig. 4) which belong to the $F = 1$ states of the protons. In addition we see the sharp line in the center of the multiplet (from the proton state $F = 0$) which does not change under the experimental conditions.

To extract the exchange-rate constant from the one-dimensional carbon spectra, a fitting routine written in the spin-simulation environment GAMMA (*33*) and using the nonlinear function minimizer MINUIT (*34*). The program diagonalizes the exchange matrices of Eqs. [15] and [17] and

TABLE 1

Results of the Computer Fits for the Exchange Spectra for Five Spinning Speeds and Six Angles θ

θ	J^{θ}_{CH}	$J^{\theta}_{CH_2}$	ν_r [kHz]	k_0 [s^{-1}][a]	$\frac{1}{T_2^{CH_2}}$ [Hz][a]	$\frac{1}{T_2^{CH}}$ [Hz][a]	k_0 [s^{-1}][a] (for a fixed linewidth of 22 Hz)
54.7°	75.8	72.7	5	28.7 ± 0.3	15.2 ± 0.1	27.0 ± 0.3	22.0 ± 0.3
			10	26.6 ± 0.5	14.8 ± 0.2	27.8 ± 0.5	19.2 ± 0.4
			15	26.2 ± 0.4	14.6 ± 0.2	29.0 ± 0.4	18.5 ± 0.3
			20	18.5 ± 0.5	15.7 ± 0.2	29.6 ± 0.4	10.6 ± 0.3
			25	27.7 ± 0.5	12.9 ± 0.2	29.4 ± 0.7	15.7 ± 0.4
40°	100.5	96.4	5	387.3 ± 6.0	27.9 ± 0.3	37.6 ± 1.4	345.0 ± 3.1
			10	206.1 ± 4.1	17.6 ± 0.3	45.7 ± 3.5	190.3 ± 2.6
			15	85.2 ± 1.5	15.2 ± 0.2	44.1 ± 1.4	92.4 ± 1.3
			20	58.3 ± 0.8	13.8 ± 0.2	43.2 ± 1.1	57.6 ± 0.8
			25	48.6 ± 0.9	12.0 ± 0.2	32.7 ± 1.2	41.8 ± 0.9
30°	113.6	109.0	5	725.3 ± 17.1	33.7 ± 0.5	37.5 ± 1.2	571.3 ± 5.7
			10	437.9 ± 11.1	20.3 ± 0.3	33.0 ± 2.7	402.1 ± 6.0
			15	300.8 ± 5.9	15.9 ± 0.2	49.1 ± 3.6	259.9 ± 3.0
			20	193.8 ± 3.3	14.4 ± 0.2	44.2 ± 3.4	176.1 ± 2.4
			25	106.2 ± 3.1	13.0 ± 0.2	48.0 ± 3.2	106.5 ± 2.4
25°	118.9	114.1	5	860.4 ± 24.2	36.0 ± 0.6	37.8 ± 1.2	646.5 ± 6.7
			10	536.1 ± 14.6	21.7 ± 0.4	30.4 ± 2.4	498.7 ± 8.1
			15	356.4 ± 7.2	16.8 ± 0.2	32.9 ± 3.4	322.2 ± 3.9
			20	255.8 ± 4.5	14.8 ± 0.2	40.8 ± 4.6	226.8 ± 3.0
			25	173.1 ± 4.9	13.3 ± 0.3	43.2 ± 4.9	157.6 ± 3.5
20°	123.3	118.3	5	987.5 ± 31.6	37.3 ± 0.6	38.5 ± 1.2	710.8 ± 7.4
			10	596.0 ± 17.1	22.8 ± 0.4	27.6 ± 2.3	567.5 ± 9.6
			15	432.2 ± 9.6	17.5 ± 0.3	32.2 ± 3.0	389.8 ± 4.9
			20	310.7 ± 5.9	14.9 ± 0.2	35.6 ± 4.7	273.7 ± 3.6
			25	217.0 ± 5.2	13.6 ± 0.3	33.7 ± 5.6	192.0 ± 4.0
0°	131.0	126.0	5	1107.8 ± 31.5	35.8 ± 0.5	36.8 ± 1.1	830.4 ± 8.5
			10	709.9 ± 11.8	21.2 ± 0.2	26.6 ± 0.7	672.9 ± 7.5
			15	497.8 ± 8.6	15.5 ± 0.2	24.5 ± 2.2	444.7 ± 4.5
			20	359.2 ± 5.3	13.3 ± 0.1	26.9 ± 3.8	306.7 ± 3.1
			25	270.7 ± 4.0	11.9 ± 0.1	26.8 ± 4.7	229.6 ± 2.9

[a] The errors indicate one standard deviation as obtained from the nonlinear fitting routine.

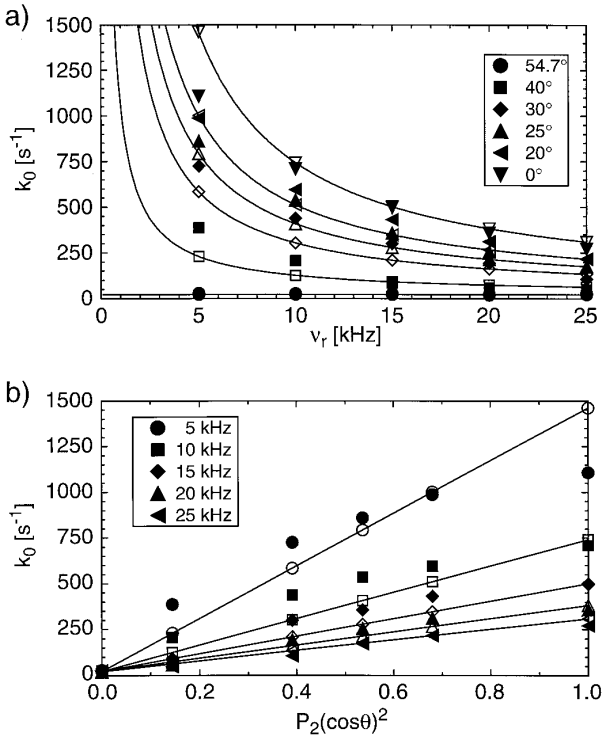

FIG. 6. (a) The exchange-rate constant k_0 as a function of the spinning speed for six measured angles θ of the effective-field orientation. The solid lines (and the open symbols) show the best fit obtained with a the function $k_0 = a/\nu_r \cdot P_2(\cos\theta)^2 + b$ for the measured data at spinning speeds of 20 and 25 kHz ($a = 7.2 \times 10^6$ s^{-2}, $b = 22$ s^{-1}) and illustrate the good agreement with the expected theoretical dependence on the spinning speed. (b) The exchange rate constant k_0 as a function of the square of the second Legendre polynomial $P_2(\cos\theta)^2$ for the five spinning speeds. The solid lines show again the best fit as in (a) and this illustrates the good agreement with the expected dependence on the angle θ. For higher spinning speeds the agreement between theoretical prediction and experimental measurements is, as expected, better. For lower spinning speeds the first-order average Hamiltonian is no longer sufficient to describe the truncation of the Hamiltonian by the MAS.

calculates the theoretical spectrum in the time domain. The program allows the simultaneous optimization of nine independent parameters—Ω_{1S}, Ω_{2S}, J^{θ}_{CH}, $J^{\theta}_{CH_2}$, k_0, k_1, k_2, $1/T_2^{CH}$, and $1/T_2^{CH_2}$—as well as the signal phases ϕ_0 and ϕ_1 and the signal amplitudes. In practice, however, usually several of these parameters were fixed to achieve faster convergence of the fitting procedure. An independent fit of the three exchange rate constants showed that k_2 was consistently at least one order of magnitude smaller than k_1 and that $k_0/k_1 \approx 0.5$, as is expected from theoretical considerations (see under Theory). For all further fits k_2 was assumed, therefore, to be zero, and the ratio of k_0 and k_1 was fixed to 1/2. In addition, the two J-couplings were fixed to their theoretical scaled values calculated from the literature values (J_{CH} = 131 Hz, J_{CH_2} = 126 Hz) (*4*) multiplied with the scaling factor due to the angle θ. This reduces the number of parameters to five—two chemical shifts, two T_2-relaxation-rate constants, and one kinetic rate constant.

Figure 5 shows two representative results of the fitting procedure (Fig. 5a for ν_r = 25 kHz and θ = 40°; Fig. 5b for ν_r = 5 kHz and θ = 20°). The experimental spectra are shown in A, the results of the nonlinear fit in B, and the residual in C. A similar high quality of agreement between the experimental data and the numerical fits was obtained for all other measurements. The numerical results of the fits for five spinning speeds from 5 to 25 kHz and for six different off-resonance decoupling angles between 54.7° and 0° are shown in Table 1.

The obtained values for the rate constant k_0 are plotted as a function of the spinning speed in Fig. 6a and as a function of the square of the second Legendre polynomial $P_2(\cos\theta)^2$ in Fig. 6b (filled symbols). In Figs. 6a and 6b, it is clearly visible that k_0 increases with increasing angle θ and decreasing spinning speed in accordance with Eq. [18]. The solid lines represent the curves of the functional form

$$k_0 = a \cdot \frac{1}{\nu_r} \cdot P_2(\cos\theta)^2 + b. \qquad [21]$$

The parameters a and b were obtained by fitting Eq. [21] to the experimental data at the spinning speeds of 20 and 25 kHz. We obtain a quite good agreement of the theoretical dependence on $P_2(\cos\theta)^2$ and ω_r^{-1} with the experimentally measured values. As expected, the agreement is better for higher spinning speeds (Fig. 6b). At lower spinning speeds the first-order average Hamiltonian (Eq. [12]) is no longer sufficient to describe the truncation of the Hamiltonian by

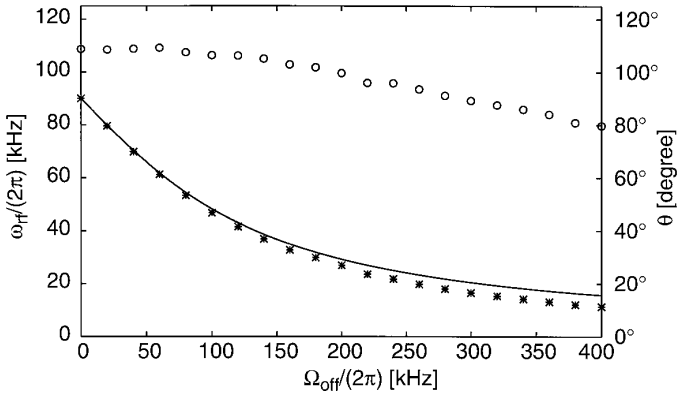

FIG. 7. Rf-field strengths (○) and angle θ (*) measured as a function of the frequency offset in a 3.2-mm Chemagnetics MAS probe between $\Omega_{off}/(2\pi)$ = 0 and 400 kHz. The rf-field strength decreases monotonically due to the change in impedance matching of the probe with increasing frequency offset. The inclination angle θ of the effective rf-field with the static magnetic field is very close to the theoretical value (solid line) which was calculated neglecting any attenuation of the rf-field as a function of the resonance offset. For higher values of the frequency offset a small correction using the calibration curve is necessary.

MAS and we have to consider higher-order terms in the average Hamiltonian expansion. The higher-order terms lead also to a deviation from the predicted $P_2(\cos\theta)^2$ scaling with the angle θ. For the magic angle, we predict $k_0 = 0$, but still measure a value of about $k_0 = 25\ s^{-1}$. The origin of these seemingly MAS-frequency-independent contributions is not completely clear.

So far, we have entirely neglected the possibility of transitions between the $F = 0$ and the $F = 1$ states of the protons in the CH_2-group. To experimentally obtain an estimate for the rate constant k_3, the magnetization was prepared selectively on the resonance line of the spin with $F = 0$ (the ''sharp'' line) using a T_2 filter, and the transfer to the exchange-broadened compound with $F = 1$ was observed. Six mixing times with τ_m between 1 ms and 2 s were measured at a spinning speed of $\nu_r = 20$ kHz (data not shown). The resulting spectra showed a sharp and a broad component which were fit with two Lorentzians. The cross-relaxation rate constant was obtained by a nonlinear fit of the system of coupled differential equations describing the relaxation process to the relative intensities of the two lines (*30–32*). The resulting cross-relaxation rate constant was $k_3 \approx 0.8\ s^{-1}$, which is in the same order of magnitude as the estimation for the theoretical value given under Theory.

CONCLUSIONS

We have demonstrated that, even at spinning speeds exceeding the proton–proton coupling by a factor of 30 and the (static) proton line width by a factor of two, proton spin diffusion is still fast enough to ''self-decouple'' the heteronuclear *J*-couplings which are in the order of $J = 125$ Hz. By scaling the homonuclear dipolar couplings through application of a strong off-resonance rf-irradiation, the effective proton–proton interaction can be scaled and the ''self-decoupling'' can be quenched. In the intermediate regime, the coalescence of the *J*-multiplet line can be observed.

From an analysis of the line shapes, the proton spin-diffusion rate constants can be determined rather accurately. The knowledge of spin-diffusion rates under MAS can be of importance for the estimation of the achievable proton spectral resolution under fast MAS and to estimate the effective size of spin systems, e.g., in a cross-polarization experiment.

APPENDIX

All measurements were carried out on a Chemagnetics Infinity CMX-400 spectrometer using a 3.2-mm double-resonance MAS probe, except for the spectra at 30 kHz, which were measured on a Chemagnetics 2.5-mm double-resonance MAS probe. All rf-fields were calibrated to 100 kHz. The carbon spectra were recorded with a simple one-pulse excitation sequence and (where mentioned) off-resonance decoupling of the protons. The spinning speed was varied from $\nu_r = 5$ to 25 kHz in 5-kHz increments. For each experiment 1024 or 2048 scans were added up with a recycle delay of 5 s.

To experimentally measure the orientation of the effective proton rf-field, a series of one-dimensional proton nutation experiments were carried out. The length of the initial pulse was incremented from 2 to 12 μs in 0.5-μs steps for offset values ranging from 0 to 400 kHz in 20-kHz steps. Each free-induction decay (FID) was fit by a damped oscillation with a variable phase. For each offset, the phase and the intensity as a function of the pulse length were used to fit the effective field strength and the two polar angles θ and ϕ which determine the orientation of the field. The important parameter for the off-resonance decoupling experiments is the inclination angle θ between the effective field and the static magnetic field, since this angle determines the scaling of the homonuclear dipolar-coupling constants. Figure 7 shows the measured rf-field strengths and the angle θ as a function of the offset. As expected, the rf-field strength decays slightly over the measured range of 400 kHz (Fig. 7). The angle θ decreases monotonically from 90° toward zero (Fig. 7). The solid line represents the theoretical value of the angle θ based on the assumption that the rf-field strength is not attenuated with increasing frequency offset. As one can see, up to an offset frequency of ca. 150 kHz this assumption is very good, while for higher offsets the effective angle has to be corrected based on the experimental measurements.

ACKNOWLEDGMENTS

Financial support from SON and the SON National HF-NMR Facility, University of Nijmegen; technical support by J. van Os, H. Janssen, and G. Nachtegaal; and scientific advice by Dr. A. P. M. Kentgens are gratefully acknowledged.

REFERENCES

1. E. R. Andrew, A. Bradbury, and R. G. Eades, *Nature (London)* **182,** 1659 (1958).
2. E. R. Andrew, A. Bradbury, and R. G. Eades, *Nature (London)* **183,** 1802 (1959).
3. I. J. Lowe, *Phys. Rev. Lett.* **2,** 285 (1959).
4. R. Aydin and H. Gunther, *Z. Naturforschung* **34b,** 528 (1979).
5. T. Terao, H. Miura, and A. Saika, *J. Chem. Phys.* **75,** 1573 (1981).
6. T. Terao, H. Miura, and A. Saika, *J. Magn. Reson.* **49,** 365 (1982).
7. K. W. Zilm and D. M. Grant, *J. Magn. Reson.* **48,** 524 (1982).
8. K. Takegoshi and C. A. McDowell, *J. Chem. Phys.* **84,** 2084 (1986).
9. A. Verhoeven, R. Verel, and B. H. Meier, *Chem. Phys. Lett.* **266,** 465 (1997).
10. N. Bloembergen, *Physica* **15,** 386 (1949).
11. H. W. Spiess, U. Haeberlen, and H. Zimmermann, *J. Magn. Reson.* **25,** 55 (1977).
12. P. Jonsen, *J. Magn. Reson.* **77,** 348–355 (1988); and *J. Magn. Reson.* **83,** 663 (1988).

13. G. Sinning, M. Mehring, and A. Pines, *Chem. Phys. Lett.* **43,** 382 (1976).

14. M. Mehring, G. Sinning, and A. Pines, *Z. Phys. B* **24,** 73 (1976).

15. M. Mehring and G. Sinning, *Phys. Rev. B* **15,** 2519 (1977).

16. H. S. Gutowsky, D. M. McCall, and C. P. Slichter, *J. Chem. Phys.* **21,** 279 (1953).

17. H. M. McConnell, *J. Chem. Phys.* **28,** 430 (1958).

18. M. Lee and W. I. Goldburg, *Phys. Rev.* **140,** A1261 (1965).

19. J. Jeener, B. H. Meier, P. Bachmann, and R. R. Ernst, *J. Chem. Phys.* **71,** 4546 (1979).

20. B. H. Meier and R. R. Ernst, *J. Amer. Chem. Soc.* **101,** 6441 (1979).

21. J. S. Waugh, L. M. Huber, and U. Häberlen, *Phys. Rev. Lett.* **20,** 180 (1968).

22. H. A. Reising, *Molec. Crystallogr.* **9,** 101 (1969).

23. J. P. Amoureux and M. B. Bee, *Mol. Phys.* **41,** 313 (1980).

24. U. Haeberlen and J. S. Waugh, *Phys. Rev.* **175,** 453 (1968).

25. U. Haeberlen, ''High Resolution NMR in Solids: Selective Averaging,'' Academic Press New York, 1968.

26. M. Mehring, ''Principles of High Resolution NMR in Solids,'' 2nd ed., Springer, Berlin, 1983.

27. R. R. Ernst, G. Bodenhausen, and A. Wokaun, ''Principles of Nuclear Magnetic Resonance in One and Two Dimensions,'' Clarendon Press, Oxford, 1987.

28. D. Suter and R. R. Ernst, *Phys. Rev. B* **32,** 5608 (1985).

29. A. Abragam, ''The Principles of Nuclear Magnetism,'' Clarendon Press, Oxford, 1961.

30. L. G. Werbelow and D. M. Grant, *J. Chem. Phys.* **63,** 544 (1975).

31. L. G. Werbelow and D. M. Grant, *J. Chem. Phys.* **63,** 4742 (1975).

32. L. G. Werbelow and D. M. Grant. Intramolecular dipolar relaxation in multispin systems, *in* ''Advances in Magnetic Resonance'' (J. S. Waugh, Ed.), Vol. 9, pp. 189–299, Academic Press, New York, 1977.

33. S. Smith, T. Levante, B. H. Meier, and R. R. Ernst, *J. Magn. Reson. A* **106,** 75 (1994).

34. The program MINUIT was used. This is part of the PACKLIB program package and was obtained under the conditions of the CERN Program Library/Division CN, CERN 1211 Geneva.